RSC Advances

PAPER

View Article Online
View Journal | View Issue

Cite this: *RSC Adv.*, 2024, **14**, 8801

Preparation, characterization, and photocatalytic performance of a PVDF/cellulose membrane modified with nano Fe_3O_4 for removal of methylene blue using RSM under visible light†

Shaghayegh Mohammadpour,[a] Peyman Najafi Moghadam[a] and Parvin Gharbani *[bc]

Received 16th December 2023
Accepted 7th March 2024

DOI: 10.1039/d3ra08599f

rsc.li/rsc-advances

In this work, a polymeric membrane-based polyvinylidene fluoride coated with cellulose and loaded with iron oxide nanoparticles (PVDF/cellulose/Fe_3O_4) was synthesized and was characterized using FESEM, XRD, AFM, and contact angle measurements. The activity and modification of the PVDF/cellulose/Fe_3O_4 membrane under visible light for the removal of methylene blue were studied using the central composite design. The effect of influential variables such as pH, methylene blue concentration, amount of Fe_3O_4 in the membrane, and irradiation time on MB removal was investigated. Analysis of variance was used to determine the significance of experimental factors and their interactions. About 72.5% methylene blue removal using the PVDF/cellulose/Fe_3O_4 membrane under visible light was achieved at optimum conditions of a pH of 9, methylene blue concentration of 600 mg L^{-1}, Fe_3O_4 amount of 0.03 g, and irradiation time of 117 min. Finally, results confirmed that the proposed membrane has good performance for methylene blue removal under visible light.

Introduction

It is very important to provide high-quality water for various industries and communities, as well as to remove and recycle toxic components from industrial wastewater.[1] The most critical pollutants of industrial wastewater are organic substances, toxins, surfactants, heavy metals, antibiotics, and dyes, which cause irreparable damage when entering the environment.[2] Various methods have been proposed for the removal of pollutants (*i.e.*, adsorption, biological, electrochemical, photocatalytic separation techniques, nanomembrane, and ultramembrane systems).[3,4] Membrane systems have been widely used due to their low energy consumption, non-pollution properties, and ease of conversion to a larger scale.[4]

New types of membranes have been prepared for water and wastewater filtration based on polymers such as polysulfone,[4] polyvinylidene fluoride,[5] polyaniline,[6] and polyacrylonitrile,[7] which have shown high efficiency in filtration. In recent years, nanocomposite membranes have expanded, enhancing the separation performance in membrane technology.[8] These membranes may show better mechanical, chemical, and thermal stability and high separation yield, high reactivity, and capacity.

Polyvinylidene fluoride (PVDF) is a fluoropolymer with repeating units of $-CH_2$ and $-CF_2$ groups. These groups create polarity on the polymer chain and allow the dissolving of the polymer in certain solvents. The arrangement of $-CF_2$ and $-CH_2$ groups along the polymer chain creates distinct properties of polymer crystal structure. The factors that directly affect the mechanical properties and resistance of the membrane include polymer crystallinity and membrane morphology. Increasing the crystallinity of PVDF causes hardness and creep resistance. Until now, PVDF/SiO_2,[9] PVDF/GeO_2,[9] PVDF/GO,[10] and nanocomposites have been prepared, but these produced composites had poor mechanical properties. Therefore, modifying materials is required to increase the mechanical properties of PVDF.

Cellulose is a carbohydrate with abundant functional groups on its surface with a high surface area.[11] These surface functional groups (C=O and C–OH) can increase the dispersion of cellulose and strengthen the intermolecular interaction with PVDF due to the extended chain composition.[12]

On the other hand, the CF groups of PVDF and the –COOH/–OH in cellulose form a hydrogen bond, leading to an all-trans TTTT conformation.[13] Also, cellulose has high thermal stability and hydrophobicity and its high thermal stability will lead to a decrease in the degree of crystalline and, as a result, a better coating on PVDF.[14] Therefore, it can be a good candidate to composite with PVDF.

[a]*Department of Organic Chemistry, Faculty of Chemistry, Urmia University, Urmia, 57153-165, Iran*

[b]*Department Chemistry, Ahar Branch, Islamic Azad University, Ahar, Iran. E-mail: parvingharbani@yahoo.com*

[c]*Industrial Nanotechnology Research Center, Tabriz Branch, Islamic Azad University, Tabriz, Iran*

† Electronic supplementary information (ESI) available. See DOI: https://doi.org/10.1039/d3ra08599f

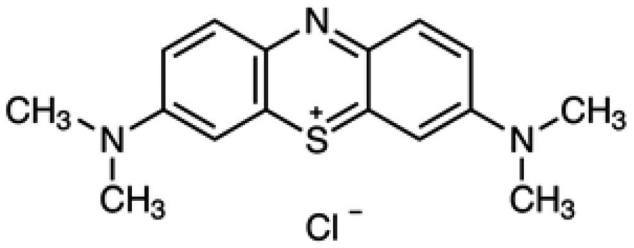

Fig. 1 Structure of methylene blue.

Research shows that the addition of nanoparticles to the polymer matrix has a positive effect on the membrane properties and can significantly improve its separation properties.[15,16] It means adding nanoparticles and metal oxides to polymer membranes is a very effective method in reducing membrane fouling and increasing the removal efficiency.[17]

Among the various nanoparticles, Fe_3O_4 is considered the most effective due to the easy preparation, exceptional conductivity, favorable magnetic properties, non-toxicity, and finally the nature of high photo responsiveness.[18] Also, Fe_3O_4 nanoparticles exhibit a high surface-to-volume ratio and show an enhanced capacity for pollutant removal.[19] The remarkable activity of Fe_3O_4 in removing environmental pollution has been proved by researchers. However, its disadvantage is the high rate of electron–hole pair recombination and agglomeration, which reduces its photo catalytic efficiency. Therefore, it should be modified in combination with other materials.[20]

The objectives of this study were to create a PVDF polymeric membrane with the addition of cellulose and nano Fe_3O_4 for the photo catalytic removal of Methylene blue (MB). In the Photo catalytic process, light was used to degrade organic pollutants.[21]

Methylene blue as a cationic dye is widely used in dyeing industries (Fig. 1). It can cause harmful effects such as eye irritation, heart palpitations, and shortness of breath in humans. Therefore, its removal from industrial wastewater has become a serious problem.[22–25]

In these membranes, the exitance of Fe_3O_4 nanoparticles improves the oxidation of Methylene Blue dye under visible light. On the other hand, the stabilization of Fe_3O_4 in the polymer matrix reduces the costs associated with conventional heterogeneous catalysis, where the nanoparticles must be recovered after use. For the optimization process, the response surface methodology (RSM) was chosen to evaluate the membrane performance. Four effective parameters *i.e.*, MB concentration, pH, amount of Fe_3O_4 in the membrane matrix, and irradiation time were used as input variables.

Table 1 Experimental factors and levels of independent variables

	Levels		
Parameter	−1	0	+1
x_1: $[MB]_0$ (mg L^{-1})	200	400	600
x_2: pH	3	6	9
x_3: $[Fe_3O_4]_0$ (g)	0.01	0.02	0.03
x_4: Irradiation time (min)	60	90	120

Materials and methods

Polyvinylidene fluoride (PVDF, Mw ~534 000 g mol^{-1}), methylene blue, cellulose (microcrystalline, powder, 20 μm) and Fe_3O_4 nanoparticles (Av = 30 nm) were prepared from Sigma-Aldrich. Dimethylformamide, HCl, NaOH and acetone were purchased from Merck Company.

Preparation of PVDF/cellulose/Fe_3O_4 membrane

1.4 g of PVDF, 10 mL of acetone, and 10 mL DMF were stirred for 20 min at 30 °C. Then 0.02 g of cellulose and 0.01, 0.02, and 0.03 g of Fe_3O_4 nanoparticles were added and stirred for 1 h at 30 °C. The obtained solution was ultrasound for 2 h. Then, the membrane-casting dope was cast on clean glass using a blade and left during the night at room temperature. The PVDF and PVDF/cellulose membranes were prepared as mentioned except without adding cellulose and Fe_3O_4, respectively. The obtained membranes were rinsed with distillate water and dried at room temperature.

Removal of methylene blue

The Box–Behnken Design (BBD) was used to design the experiments and produce the quadratic model of the process. Variables including MB concentration (*A*), pH (*B*), Fe_3O_4 amount in the membrane matrix (*C*) and irradiation time (*D*) were selected (Table 1).

Using variables at three levels, twenty-nine experiments were designed. The photocatalytic performance of the prepared membrane was performed in a batch system that included a crystallizer with a volume of 100 mL containing MB solution and Xe lamp ($\lambda > 420$ nm) as a light source which was located on top of the wooden box. The membrane was cut into small pieces (2 cm^2) and was added to the dye solution in a wooden box on a stirrer. The pH of the MB solution was determined using HCl and NaOH solutions. At certain time intervals, 5 mL of the solution was collected for analysis by UV-vis spectrophotometer, model DR5000-15V (HACH Co, America) at 434 nm. The

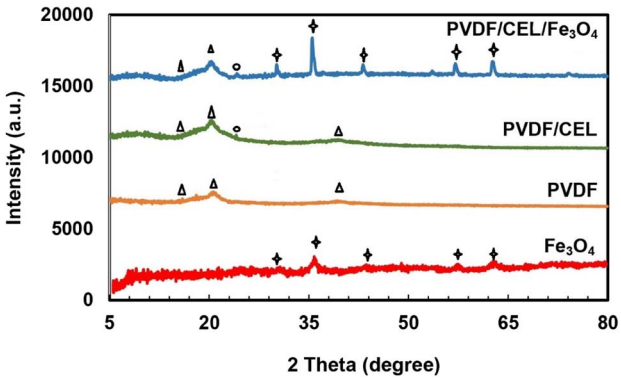

Fig. 2 XRD of Fe_3O_4, PVDF, PVDF/cellulose and PVDF/cellulose/Fe_3O_4.

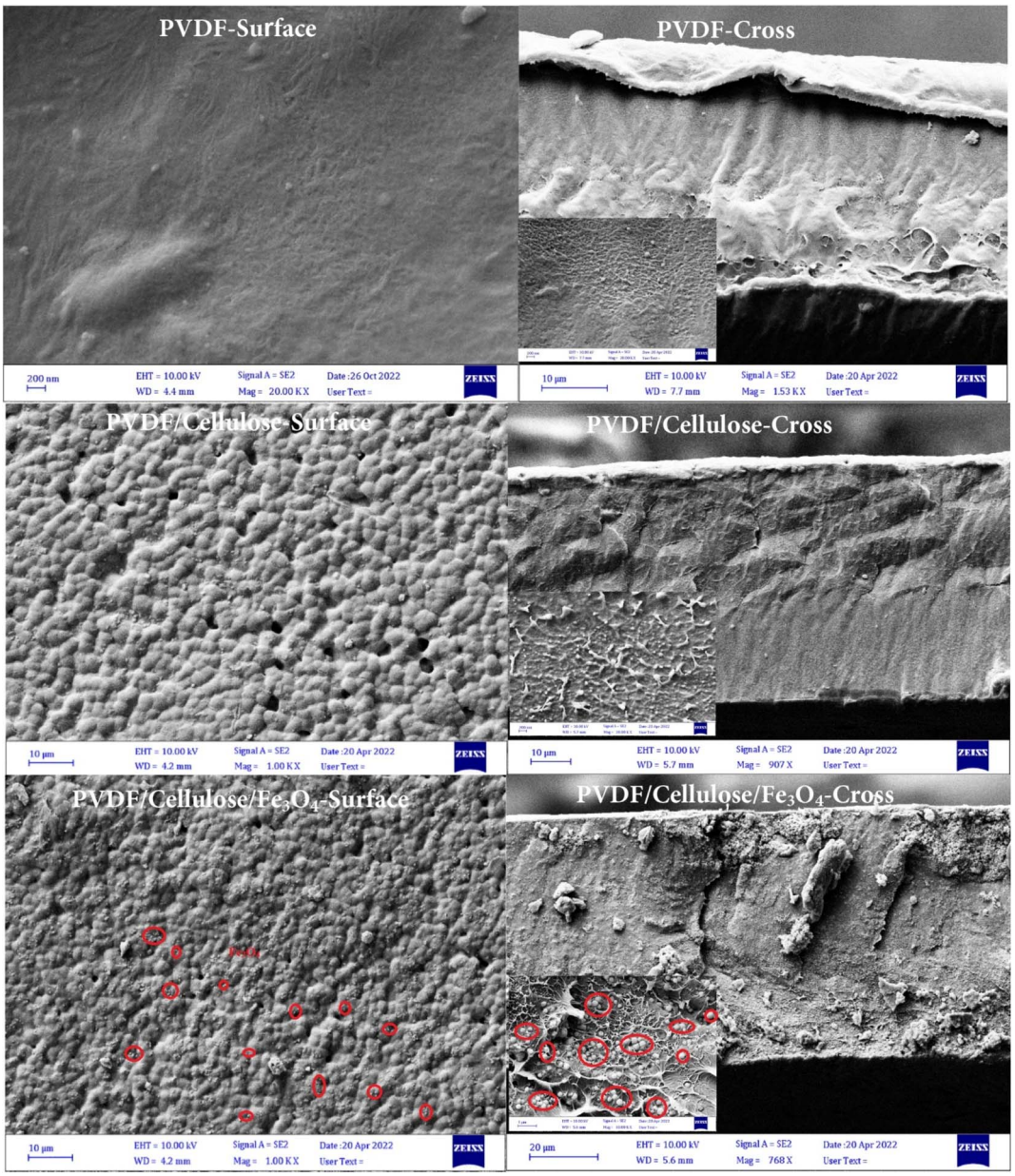

Fig. 3 FESEM images of surface and cross-section of PVDF, PVDF/cellulose and PVDF/cellulose/Fe_3O_4 membranes.

photocatalytic degradation of MB was obtained using the following equation (eqn (1)).[26]

$$R(\%) = \frac{[C]_0 - [C]_t}{[C]_0} \times 100 \quad (1)$$

$[C]_0$ and $[C]_t$ are initial and at any time concentrations of MB (mg L^{-1}), respectively.

Results and discussion

Characterization

XRD analysis was used to study the crystal structure of synthesized samples.[27] X-ray diffraction patterns of Fe_3O_4, PVDF, PVDF/cellulose, and PVDF/cellulose/Fe_3O_4 membranes are shown in Fig. 2. In the XRD pattern of Fe_3O_4, an observed peak at 35.71° (3 11) belongs to a crystal plane. Other peaks appeared at $2\theta = 30.31°$ (2 0 0), 43.37° (4 0 0), 57.39° (5 1 1), and 62.86° (4 0 0) according to JCPDS Card No. 19-0629.[28] In the XRD pattern of PVDF, three peaks appear around $2\theta = 18.04$, 20.65, and 36.4° correspond to the crystalline peaks (021), (110), and (020) of PVDF crystalline phase,[6] respectively. Standard XRD patterns of cellulose, Fe_3O_4 and PVDF is shown in Fig. 2. In the XRD of the PVDF/cellulose, in addition to the peaks of PVDF, a peak is seen at $2\theta = 22°$, which is related to the crystalline phase (001) of cellulose that emphasizes the presence of cellulose.[13] The presence of peaks appearing at $2\theta = 30.16$, 57, and 63° in the XRD of PVDF/cellulose/Fe_3O_4 confirms the presence of pure Fe_3O_4 with a spinel structure. The peaks of PVDF and cellulose can also be seen.

Analysis Result		
Sample	**Contact angle**	**Picture**
PVDF	**77±4**	
PVDF/Cellulose	**61±3**	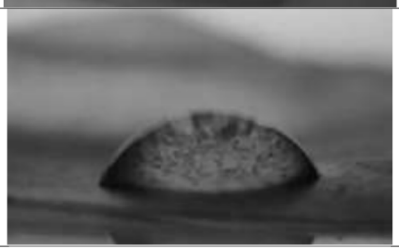
PVDF/Cellulose/Fe_3O_4	**87±5**	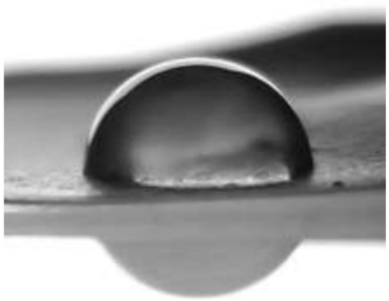

Fig. 4 Contact Angle of PVDF, PVDF/cellulose and PVDF/cellulose/Fe_3O_4 membranes.

FESEM analysis was used to evaluate the morphology of prepared membranes.[29] Fig. 3 shows the FESEM images of the surface and cross-section of prepared membranes. The surface image of the PVDF membrane shows a relatively dense membrane, while its cross-sectional image shows a relatively non-uniform structure. The surface image of the PVDF/cellulose membrane shows a very uniform and porous surface, which confirms that the addition of cellulose has made the relatively uniform surface of the PVDF. The cross-sectional image of PVDF/cellulose shows that cross-links are formed. After adding Fe_3O_4 nanoparticles to the PVDF/cellulose membrane, the Fe_3O_4 nanoparticles (red pen) are uniformly distributed on the surface of the PVDF/cellulose membrane. The cross-sectional FESEM image clearly shows the dispersion of Fe_3O_4 spherical nanoparticles on the membrane.

Contact Angle (CA) measurement is a simple method to obtain and collect information about the hydrophobicity/hydrophilicity of the membranes. The contact angle of the outer surface of the membranes was measured before and after the coating (Fig. 4). As seen, the contact angles of the PVDF, PVDF/cellulose, and PVDF/cellulose/Fe_3O_4 membranes are about 77, 61, and 87. The contact angle decreases slightly with the increase of cellulose concentration, while it increases slightly with the dispersion of Fe_3O_4 nanoparticles on PVDF/cellulose. However, it can be concluded that all three membranes are hydrophile and the dispersion of Fe_3O_4 nanoparticles on the PVDF/cellulose membrane slightly decreases the hydrophilicity of the membrane.

AFM analysis was used to evaluate the surface morphology and roughness of membranes.[29] Root mean square (RMS) was obtained from the AFM images. The thickness, average roughness (R_a), and RMS roughness of prepared membranes are presented in Table 2. As seen, the R_a values for PVDF,

Table 2 Thickness, average roughness (R_a) and root mean square roughness (RMS) of prepared membranes

Membrane	Thickness (μm)	RMS (nm)	R_a (nm)
PVDF	162.1	40.83	32.92
PVDF/cellulose	796.3	180.4	141.3
PVDF/cellulose/Fe_3O_4	1818	384.0	311.7

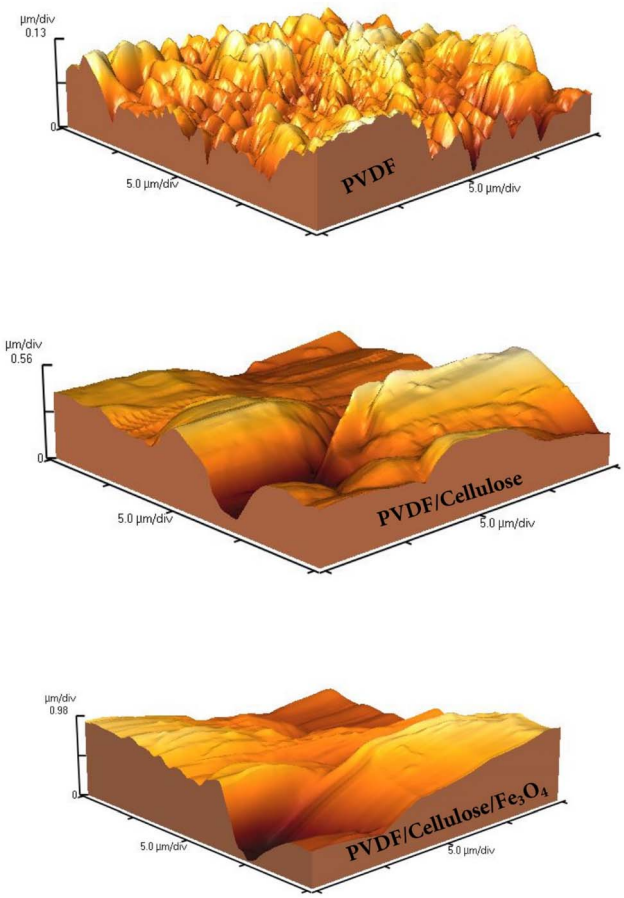

Fig. 5 AFM of PVDF, PVDF/cellulose, and PVDF/cellulose/Fe_3O_4.

PVDF/cellulose, and PVDF/cellulose/Fe_3O_4 were obtained at 32.92, 141.3, and 311.7 nm, respectively. Likewise, the RMS values for PVDF, PVDF/cellulose and PVDF/cellulose/Fe_3O_4 were obtained at about 40.83 nm, 180.4 nm, and 384 nm, respectively. The results confirm that the roughness of the PVDF membrane increased with the addition of cellulose and Fe_3O_4 nanoparticles due to increasing the viscosity of the solution.[5] It is important to state that the contact angle between the water drop and the surface of the material in addition to the hydrophilicity of the surface, also depends on its roughness. The results show that the addition of mineral particles into the polymer matrix increases the surface roughness. The results of AFM analysis for prepared membranes are shown in Fig. 5.

Optical properties. The optical absorption property is one of the most important factors in evaluating the photocatalytic performance of a material.[30,31] UV-vis analysis was used to study the optical absorption properties and determine the band gap of the membrane. Fig. 6 shows the UV-vis spectrum and the Tauc plots of the synthesized membrane. As can be seen, the compounds have an absorption in the UV-vis region (Fig. 6a), and band gap for cellulose, PVDF, Fe_3O_4 and PVDF/cellulose/Fe_3O_4 were found to be around 3.1, 2.35, 2.6 and 1.9 eV, respectively (Fig. 6b).

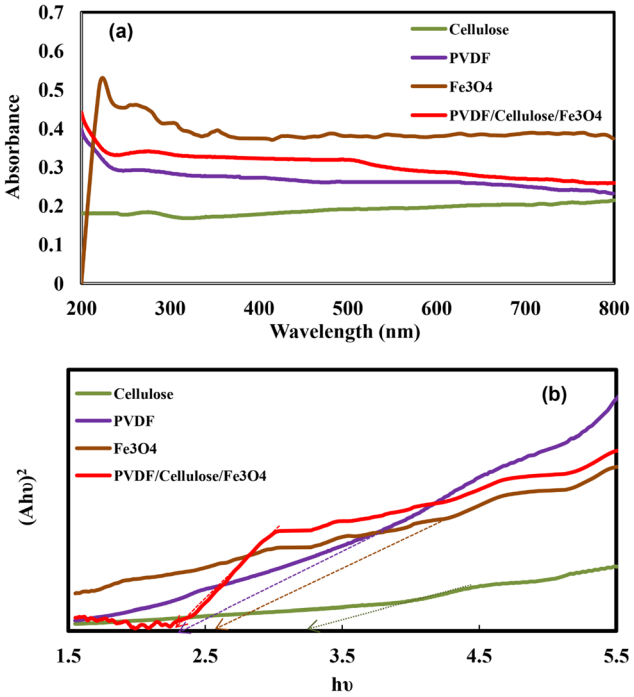

Fig. 6 (a) UV-visible, (b) Taut plots of cellulose, PVDF, Fe_3O_4 and PVDF/cellulose/nana Fe_3O_4.

Recombination of electron–hole pairs in semiconductors releases energy in the form of photoluminescence (PL), and lower PL intensity indicates a lower carrier recombination rate, which leads to efficient photocatalytic activity.[32]

The intensity of the PL spectrum depends on the rate of recombination of electron–hole pairs and PL spectroscopy is used to investigate photogenerated electron–hole trapping, migration, and transport. Fig. 7 shows the photoluminescence (PL) of cellulose, PVDF, Fe_3O_4 and PVDF/cellulose/nana Fe_3O_4 with an excitation wavelength of 320 nm. The low PL intensity of PVDF/cellulose/nana Fe_3O_4 indicates more separation of photogenerated electron–hole pairs, which is very satisfactory for efficient photocatalytic performance. Therefore, the decrease in electron–hole recombination rate leads to high photocatalytic activity.[33]

Box–Behnken Design (BBD) and statistical analysis

Under the design conditions and various experiments proposed by the RSM (Table 3), the removal percentage of MB increases from 52.55 to 76.44%.

A polynomial mathematical equation showing the obtained R%, as a function of MB concentration (A), pH (B), Fe_3O_4 nanoparticles amount in the membrane matrix (C), and irradiation time (D) is revealed using eqn (2).

$$R = 64.7 - 1.58 \times A + 7.7 \times B + 4.7 \times C + 3.36 \times D - 0.9 \times A \times B + 0.03 \times A \times C0.12 \times A \times D + 0.31 \times B \times C + 0.048 \times B \times D - 0.13 \times C \times D - 0.63 \times A^2 - 0.49 \times B^2 - 0.18 \times C^2 - 0.17D^2 \quad (2)$$

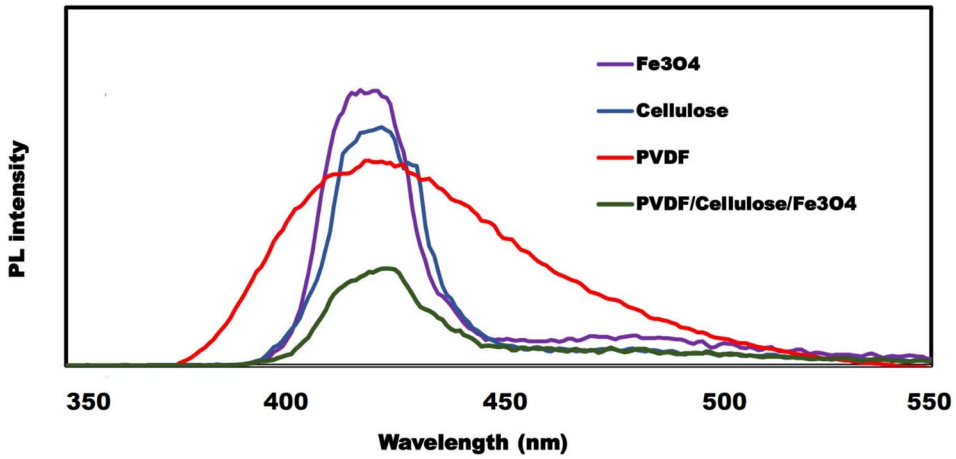

Fig. 7 Photoluminescence of cellulose, PVDF, Fe_3O_4 and PVDF/cellulose/nana Fe_3O_4.

Table 3 BBD design matrix for three variables with experimental values for MB degradation

	Parameter values				Removal (%)
Run	x_1	x_2	x_3	x_4	Exp.
1	400	6	0.03	60	65.53
2	400	6	0.02	90	65.55
3	200	6	0.02	120	69.00
4	200	6	0.03	90	70.71
5	400	9	0.02	120	74.93
6	600	6	0.02	120	65.65
7	400	6	0.02	90	64.33
8	600	6	0.03	90	66.64
9	200	3	0.02	90	54.61
10	400	3	0.01	90	52.55
11	400	6	0.01	120	62.40
12	400	3	0.02	60	53.95
13	200	6	0.02	60	62.22
14	400	6	0.03	120	72.16
15	600	6	0.02	60	59.36
16	400	6	0.01	60	55.25
17	400	3	0.02	120	60.59
18	400	6	0.02	90	64.03
19	400	9	0.01	90	66.53
20	600	9	0.02	90	69.72
21	400	3	0.03	90	61.22
22	200	6	0.01	90	61.90
23	600	3	0.02	90	54.18
24	400	9	0.02	60	68.10
25	200	9	0.02	90	73.76
26	400	6	0.02	90	64.94
27	600	6	0.01	90	57.71
28	400	6	0.02	90	64.63
29	400	9	0.03	90	76.44

Analysis of variance (ANOVA)

ANOVA was used as a statistical method to analyze the responses. R^2 and R^2 Adj determined the quality of the presented polynomial model. The results of ANOVA and multiple regression coefficients of MB removal are tabulated in Table 4. The significance and influence of each independent variable were determined using *F*-values. The practicability and statistical significance results were confirmed using prob > *F*. In general, a significance level of 0.05 is considered in RSM.[34] In this research, the upper *F* value of 88.38 and $p < 0.0001$ expresses the significance of the model ($F <$ prob less than 0.05 indicates that the model is statistically significant), and the results show that the model can explain the percentage of MB removal. On the other hand, the lack of fit (LOF) of 0.1245 indicates that the regression equation can be used to explain the relationship between the response variables and the removal percentage. According to the *p*-value of the independent variables, the variables *A*, *B*, *C*, and *D* are statistically significant ($p < 0.05$), while, *AC*, *AD*, *AB*, *BC*, *BD*, *CD*, A^2, B^2, C^2, and D^2 are not significant ($p > 0.05$). The high value of the linear regression coefficient R^2 (0.9888) and R^2 adjusted (0.9776) indicate a good performance of the model. Notably, R^2 of 0.9888 indicates that more than 98.88% of the changes in the response function can be justified by the obtained model. In other words, the regression model is statistically significant. Adeq precision of 35.77 > 4 indicates the signal-to-noise ratio was desirable for the model. Parallel to these results, the relatively low value of CV% = 1.5 for variables confirms the accuracy of the measurements and the reliability of the tests. Std dev. of 0.96 and press of 69.12 indicate the matching of the model with the experimental results.

Effect of the variables as a response surface and 3D plots

To study the interaction of variables, three-dimensional (3D) plots were used. The effect of the input parameters on the response variable is shown in Fig. 8. This figure shows that increasing the initial concentration of the MB, irradiation time, the amount of Fe_3O_4 in the membrane, and the pH leads to an increase in MB removal.

The pH of the solution is one of the important parameters in the photocatalytic process, which affects the charge of active sites available on the membrane surface. As can be seen in Fig. 8a, the prepared membrane is more effective in an alkaline solution. At high pH values, the surface of the membrane is negatively charged and since the MB is a cationic dye, significant electrostatic interaction with the positively charged MB and negatively charged

Table 4 Analysis of Variance

Sum of			Mean	*F*	*p*-Value
Source	Squares	Df	Square	Value	Prob > *F*
Model	1148.52	14	82.04	88.38	< 0.0001
A-concentration	29.88	1	29.88	32.19	< 0.0001
B-pH	711.14	1	711.14	766.1	< 0.0001
C-Fe_3O_4	264.71	1	264.71	285.16	< 0.0001
D-time	135.5	1	135.5	145.98	< 0.0001
AB	3.25	1	3.25	3.51	0.0822
AC	3.58×10^{-3}	1	3.58×10^{-3}	3.86×10^{-3}	0.9513
AD	0.062	1	0.062	0.067	0.8
BC	0.38	1	0.38	0.41	0.5308
BD	9.35×10^{-3}	1	9.35×10^{-3}	0.01	0.9215
CD	0.069	1	0.069	0.074	0.7898
A^2	2.57	1	2.57	2.77	0.1182
B^2	1.56	1	1.56	1.68	0.2155
C^2	0.21	1	0.21	0.23	0.6417
D^2	0.18	1	0.18	0.2	0.6651
Residual	13	14	0.93		
Lack of fit	11.63	10	1.16	3.41	0.1245
Pure error	1.37	4	0.34		
Cor total	1161.52	28			
Std dev.	0.96	*R*-squared	0.9888		
Mean	64.09	Adj. *R*-squared	0.9776		
C.V. %	1.5	Pred. *R*-squared	0.9405		
Press	69.12	Adeq. precision	35.776		

membrane is obtained.[35] Also, the produced hydroxyl radicals can enhance the MB removal at higher pHs.

Increasing the initial concentration of MB has a positive effect on MB removal efficiency (Fig. 8a). In fact, increasing the initial concentration of MB provides a higher driving force to overcome all existing resistances in MB mass transfer between the surface membrane and liquid phase. Fig. 8b shows that Fe_3O_4 increasing in the membrane has an affirmative effect on MB removal. The photogenerated electrons and holes from the conduction and valence band of Fe_3O_4 participate in the degradation process.[36] Also, since OH radicals are generated and react in the vicinity of Fe_3O_4, it is important that MB molecules can attach to the Fe_3O_4 surface for the catalytic reaction to occur. It can be stated that MB molecules are adsorbed first on Fe_3O_4 active catalytic sites and then oxidized by photo-induced OH radicals. Under visible light, Fe_3O_4 is excited, electrons and holes are generated, and MB degradation is enhanced.[37] Also, Fig. 8b illustrates irradiation time on the removal of MB under visible light. The increase in MB removal with increasing irradiation time can be related to more MB adsorption and more Fe_3O_4 oxidation on the surface of the membrane with increasing time.

Optimization

The main goal of the experiment design is to achieve the optimal values of the variables for the MB removal. The optimization results indicate that about 72.5% of MB is removed

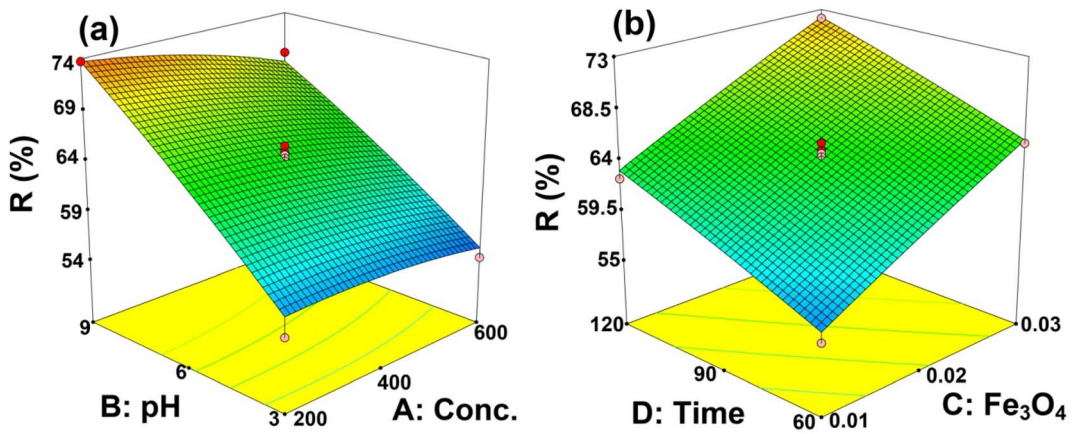

Fig. 8 3D plots of (a) pH and MB concentration; (b) time and Fe_3O_4 amount interactions.

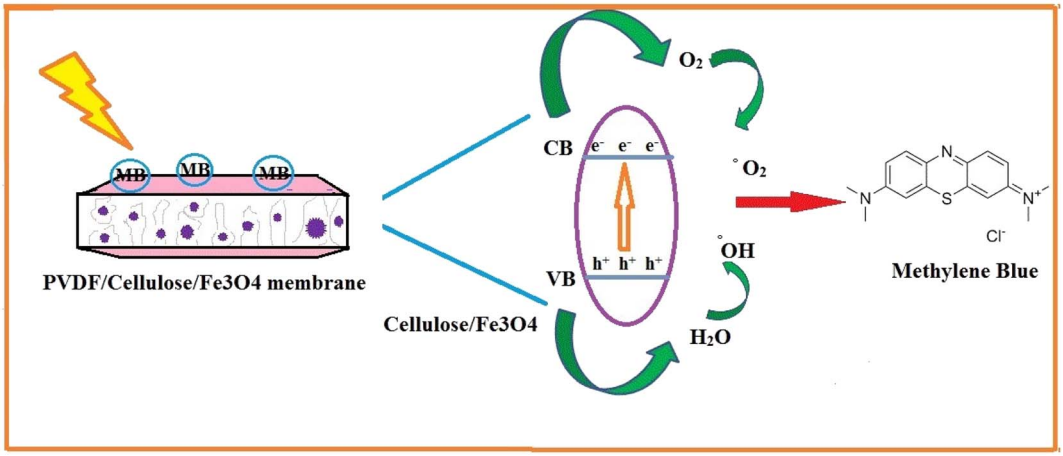

Fig. 9 Proposed mechanism of MB photo degradation by PVDF/cellulose/nano Fe_3O_4 membrane.

Table 5 Photo catalysis performance comparison of methylene blue removal based on Fe_3O_4 photocatalyst

Photocatalyst	Pollutant	% removal	Ref
Fe_3O_4-MWCNTs	Methylene blue	98.46	40
Fe_3O_4@Ag@TiO_2	Methylene blue	79.91	41
r-GO-Fe_3O_4	Methylene blue	98.38	42
δ-Fe_3O_4@GO	Methylene blue	90.6	43
Fe_3O_4@SiO_2 @TiO_2	Methylene blue	97.0	44
GO-$LaFeO_3$	Methylene blue	91.21	45
Fe_3O_4@SiO_2	Methylene blue	94.83	46
Fe_3O_4@SiO_2 @TiO_2	Methylene blue	94.8	47
Fe_2O_3/graphene/CuO	Methylene blue	94.27	48
Fe_3O_4@C@Ru	Methylene blue	92.71	49
PVDF/cellulose/Fe_3O_4	Methylene blue	72.50	This paper

with PVDF/cellulose/Fe_3O_4 membrane at a pH of 9, MB concentration of 600 mg L^{-1}, and 0.03 g of Fe_3O_4 at 117 min.

Proposed mechanism. Fig. 9 shows the proposed membrane mechanism for MB degradation. Firstly, with light irradiation, the valence electrons are transferred to the conduction band (CB). As soon as the excited electrons reach the conduction band, they easily move to the cellulose surface and photo-generated electron–hole pairs are formed. Then, the obtained electrons react with dissolved oxygen in water and form superoxide and hydroxyl free radicals. These superoxide and free radicals degrade MB into less toxic substances.[38,39]

Table 5 shows the photo degradation efficiency of MB removal compared with other Fe_3O_4-based photocatalyst.

As seen in Table 5, the efficiency of PVDF/cellulose/nano Fe_3O_4 membrane on removal of MB in comparison to others is lower. In contrast, other photocatalysts need to recover after usage but in the case of this membrane, there is no need to recover the photocatalyst after the removal of MB.

Conclusion

In this research, PVDF/cellulose/Fe_3O_4 membrane was synthesized and analyzed using XRD, FESEM, AFM, and contact angle measurement (CA). The design of experiments was done using response surface methodology and modeling and optimization of operational parameters were carried out. The results showed that the increase of pH, irradiation time, MB concentration, and amount of Fe_3O_4 in the membrane had an affirmative effect on the MB removal. Therefore, the PVDF/cellulose/Fe_3O_4 membrane is an efficient membrane for removing MB under visible light. Also, the RSM has a good agreement with being able to provide a suitable model for the removal of MB, and the percentage of predicted removal of MB is in good agreement with the experimental results.

Data availability

All data generated or analysed during this study are included in this published article (and its ESI† files).

Author contributions

Parvin Gharbani: conceptualization, methodology, formal analysis, writing – review & editing. Peyman Najafi Moghadam: funding acquisition, project administration, writing – review & editing. Shaghayegh Mohammadpour: methodology.

Conflicts of interest

The authors declare that there is no conflict of interest.

References

1 A. Mehrizad, M. Aghaie, P. Gharbani, S. Dastmalchi, M. Monajjemi and K. Zare, *J. Environ. Health Sci. Eng.*, 2012, **9**, 1–6.
2 H. Sun, L. Wang, F. Guo, Y. Shi, L. Li, Z. Xu, X. Yan and W. Shi, *J. Alloys Compd.*, 2022, **900**, 163410–163423.
3 Z. Xu, Y. Shi, L. Li, H. Sun, M. S. Amin, F. Guo, H. Wen and W. Shi, *J. Alloys Compd.*, 2022, **895**, 162667–162678.
4 S. Gasemloo, M. R. Sohrabi, M. Khosravi, S. Dastmalchi and P. Gharbani P, *Water Sci. Technol.*, 2016, **14**, 2611–2619.

5 P. Hassanzadeh, P. Gharbani, F. Derakhshanfard and B. M. Maher, *J. Polym. Environ.*, 2021, 1–10.
6 M. Beheshtikya and P. Gharabani, *J. water wastewater*, 2019, 61–72.
7 N. Scharnagl N and H. Buschatz, *Desalination*, 2001, **139**, 191–198.
8 S. Sorribas, P. Gorgojo, C. Téllez, J. Coronas and A. G. Livingston, *J. Am. Chem. Soc.*, 2013, **135**, 15201–15208.
9 E. Kar, N. Bose, S. Das, N. Mukherjee and S. Mukherjee, *Phys. Chem. Chem. Phys.*, 2015, **17**, 22784–22798.
10 P. Gharbani, A. Mehrizad and I. Jafarpour, *Pol. J. Chem. Technol.*, 2015, **17**, 95–99.
11 J. E. Lee, Y. E. Shin, G. H. Lee, J. Kim, H. Ko and H. G. Chae, *Composites, Part B*, 2021, **223**, 109098.
12 B. Ma, J. Yang, Q. Sun, W. Jakpa, X. Hou and Y. Yang, *J. Mater. Sci.*, 2017, **52**, 9946–9957.
13 Y. Li, Q. Hu, R. Zhang, W. Ma, S. Pan, Y. Zhao, Q. Wang and P. Fang, *Materials*, 2022, **10**, 7026.
14 M. Li, B. Jiang, S. Cao, X. Song, Y. Zhang, L. Huang and Q. Yuan, *RSC Adv.*, 2023, **13**, 10204–10214.
15 J.-E. Lee, Y.-E. Shin, G.-H. Lee, J. Kim, H. Ko and H. G. Chae, *Composites, Part B*, 2021, **223**, 109098.
16 E.-S. Kim, Y. Liu and M. G. El-Din, *J. Membr. Sci.*, 2013, **429**, 418–427.
17 Y. Zhao, Z. Xu, M. Shan, C. Min, B. Zhou, Y. Li, B. Li, L. Liu and X. Qian, *Sep. Purif. Technol.*, 2013, **103**, 78–83.
18 P. Mishra, S. Patnaik and K. Parida, *Catal. Sci. Technol.*, 2019, **9**, 916–941.
19 P. Mishra, A. Behera, D. Kandi, S. Ratha and K. Parida, *Inorg. Chem.*, 2020, **59**, 4255–4572.
20 D. K. Padhi, T. K. Panigrahi, K. Parida, S. K. Singh and D. P. Mishra, *ACS Sustain. Chem. Eng.*, 2017, **5**, 10551–10562.
21 A. Mehrizad and P. Gharbani, *Prog. Color, Color. Coat.*, 2016, **9**(2), 135–143.
22 S. Nayak, K. K. Das and K. Parida K, *J. Colloid Interface Sci.*, 2023, **634**, 121–137.
23 W. Shi, H. Chenchen, S. Yuxing, F. Guo and Y. Tang, *Sep. Purif. Technol.*, 2023, **304**, 122337–122340.
24 D. K. Padhi, K. M. Parida and S. K. Singh, *J. Environ. Chem. Eng.*, 2016, **4**, 3498–3511.
25 J. Pan, L. Wang, Y. Shi, L. Li, Z. Xu, H. Sun, F. Guo and W. Shi, *Sep. Purif. Technol.*, 2022, **284**, 120270–120280.
26 S. Nayak, G. Swain and K. Parida, *ACS Appl. Mater. Interfaces*, 2019, **11**, 20923–20942.
27 K. K. Das, D. P. Sahoo, S. Mansingh and K. Parida, *ACS Omega*, 2021, **6**, 30401–30418.
28 S. Mansingh, D. K. Padhi and K. Parida, *Appl. Surf. Sci.*, 2019, **466**, 679–690.
29 F. Guo, Z. Chen, X. Huang, L. Cao, X. Cheng, W. Shi and L. Chen, *Sep. Purif. Technol.*, 2021, **275**, 119223–119233.
30 K. K. Das, S. Patnaik, B. Nanda, A. C. Pradhan and K. Parida, *ChemistrySelect*, 2019, **4**, 1806–1819.
31 K. K. Das, S. Patnaik, S. Mansingh, A. Behera, A. Mohanty, C. Acharya and K. M. Parida, *J. Colloid Interface Sci.*, 2020, **561**, 551–567.
32 X. Sun, K. He, Z. Chen, H. Yuan, F. Guo and W. Shi, *Sep. Purif. Technol.*, 2023, **324**, 124600.
33 K. K. Das, S. Mansingh, R. Mohanty, D. P. Sahoo, N. Priyadarshini and K. Parida, *J. Phys. Chem. C*, 2022, **127**, 22–40.
34 P. Gharbani, *J. Mol. Liq.*, 2017, **242**, 229–234.
35 X. Lin, X. Wang, Q. Zhou, C. Wen, S. Su, J. Xiang, P. Cheng, X. Hu, Y. Li and X. Wang, *ACS Sustain. Chem. Eng.*, 2018, **7**, 1673–1682.
36 W. Shi, H. Chenchen, F. Yongming, G. Feng, T. Yubin and Y. Xu, *J. Chem. Eng.*, 2022, **433**, 133741–133744.
37 P. Gharbani, A. Mehrizad and S. A. Mosavi, *npj Clean Water*, 2022, **5**(1), 34.
38 S. Mansingh, S. Sultana, R. Acharya, M. K. Ghosh and K. M. Parida, *Inorg. Chem.*, 2020, **59**, 3856–3873.
39 L. Chen, J. Wang, X. Li, C. Zhao, X. Hu, Y. Wu and Y. He, *Inorg. Chem. Front.*, 2022, **9**, 2714–2722.
40 S. Hussain, M. D. Alam, M. Imran, M. A. Ali, T. Ahamad, A. S. Haidyrah, S. M. A. Raji Alotaibi and M. Shariq, *Alexandria Eng. J.*, 2022, **61**(11), 9107–9117.
41 W. J. Tseng, Y.-C. Chuang and Y.-A. Chen, *Adv. Powder Technol.*, 2018, **29**(3), 664–671.
42 M. Imran, M. M. Alam, S. Hussain, M. A. Ali, M. Shkir, A. Mohammad, T. Ahamad, A. Kaushik, K. Irshad, M. M. Alam, S. Hussain, M. A. Ali, M. Shkir, M. Akbar, T. Ahamad, A. Kaushik and K. Irshad, *Ceram. Int.*, 2021, **47**(22), 31973–31982.
43 A. Rehman, A. Daud, M. F. Warsi, I. Shakir, P. O. Agboola, M. I. Sarwar and S. Zulfiqar, *Mater. Chem. Phys.*, 2020, **256**, 123752.
44 C. I. Tarcea, C. M. Pantilimon, E. Matei, A. M. Predescu, A. C. Berbecaru, M. Rapa, A. Turcanu and C. Predescu, *IOP Conf. Ser.: Mater. Sci. Eng.*, 2020, **877**, 012008.
45 M. A. Mutalib, F. Aziz, N. A. Jamaludin, N. Yahya, A. F. Ismail, M. A. Mohamed, M. Z. M. Yusop, W. N. W. Salleh, J. Jaafar and N. Yusof, *Korean J. Chem. Eng.*, 2018, **35**(2), 548–556.
46 S. Dagher, A. Soliman, A. Ziout, N. Tit, A. Hilal-Alnaqbi, S. Khashan, F. Alnaimat and J. Abu Qudeiri, *Mater. Res. Express*, 2018, **5**(6), 065518–065531.
47 Í. L. Fernandes, D. Pereira Barbosa, S. Botelho de Oliveira, V. Antônio da Silva, M. Henrique Sousa, M. Montero-Muñoz and J. A. H. Coaquira, *Appl. Surf. Sci.*, 2022, **580**, 152195.
48 P. Nuengmatcha, P. Porrawatkul, S. Chanthai, P. Sricharoen and N. Limchoowong, *J. Environ. Chem. Eng.*, 2019, **7**, 103438.
49 Q. Zhang, L. Yu, C. Xu, J. Zhao, H. Pan, M. Chen, Q. Xu and G. Diao, *Appl. Surf. Sci.*, 2019, **483**, 241–251.